Topological edge states of Kekulé-type photonic crystals induced by a synchronized rotation of unit cells

Rui Zhou,[1] Hai Lin [●],[1,*] Y. Liu (刘泱杰) [●],[2,†] Xintong Shi,[1] Rongxin Tang,[3] Yanjie Wu,[1] and Zihao Yu[1]

[1]*College of Physics Science and Technology, Central China Normal University, Wuhan 430079, Hubei Province, China*
[2]*School of Physics and Electronic Sciences, Hubei University, Wuhan 430062, Hubei Province, China*
[3]*Institute of Space Science and Technology, Nanchang University, Nanchang 330021, Jiangxi Province, China*

Generating and manipulating Dirac points in artificial atomic crystals has received attention, especially in photonic systems due to their ease of implementation. In this Letter, we propose a two-dimensional photonic crystal made of a Kekulé lattice of pure dielectrics, where the internal rotation of cylindrical pillars induces optical Dirac-degeneracy breaking. Our calculated dispersion reveals that the synchronized rotation reverses bands and switches parity as well so as to induce a topological phase transition. Our simulation demonstrates that such topologically protected edge states can achieve robust transmission in defect waveguides under deformation, and therefore provides a pragmatically tunable scheme to achieve reconfigurable topological phases.

I. INTRODUCTION

In the past decades, topological photonics has become a rapidly developing research field that aims to explore the wave physics of topological phases of matter in analog. The concept of topological insulators in condensed matter physics has been used in many wave physics fields [1,2]. Haldane and Raghu [3,4] first brought the quantum Hall effect (QHE) to the field of photonics and theoretically proved the photonic quantum Hall effect (PQHE), which opened new avenues for topologically protected optical transmission devices (such as topological lasers, waveguides, and quantum circuits) [5,6]. The topological edge states generated on the interface between different topological phases promise fascinating features such as robust transmission, backscattering suppression, and defect immunity. Topological photonic devices enabling edge state transmission have brought unprecedented opportunities in controlling the electromagnetic (EM) waves at the microwave and optical frequency bands [3,5,7].

The first realization of a photonic topological state was based on the microwave platform of gyromagnetic photonic crystals by applying a magnetic field to break the time-reversal (TR) symmetry of the system [8,9]. However, a weak gyromagnetic effect hinders their extension towards higher-frequency bands and more manipulative scenarios. To sidestep this issue, all-dielectric photonic crystals (PCs) with judiciously designed unit cells have been proposed [3,10] to achieve topological phases through adjusting the geometrical structures in the primitive cell of all-dielectric PCs with C_6 symmetry [11–14]. Floquet insulators, the valley Hall effect, and the photonic quantum spin Hall effect (PQSHE) have been realized both in theory and in experiment [3,15–17].

The PCs with C_6 symmetry including circular pillars (dielectric cylinders or pores), core shells (circular rings), and elliptical dielectric cylinder clusters were proposed to achieve quantum spin Hall (QSH) effects [3,15,18]. At the interface between different topological phases, the helical edge states are sandwiched which lead to unidirectional nonscattering propagation. This unique robust feature can be used to realize band-gap devices such as topology lasers, integrated optical circuits, etc. [15,19–21].

In this Letter, we propose an internal rotating mechanism to achieve topological edge states via sandwiching two distinct topological phases, on a two-dimensional PC made of a Kekulé lattice in dielectrics [3,15,16,22]. This proposal provides a flexible way to achieve optical topological phase transitions. The physical principle is, by the internal rotation, that a crystal lattice with C_{6v} symmetry (representing sixfold rotational symmetry and mirror symmetry in six different directions) becomes C_6 [23]. Destruction of the mirror symmetry of the lattice causes the Dirac point Γ to break its degeneracy. The generation and breaking of the Dirac degeneracy result in the occurrence of topological phase transitions [22]. At the interface of different topological phases generated in this manner, we observe in simulation the edge states protected by the pseudo-time-reversal (TR) [23,24] symmetry accompanied by C_6 symmetry. As a merit of that, we also design a bent waveguide and a defected one and observe in simulation that even in the presence of sharp turns or defects, these edge states still propagate robustly.

II. THEORY AND MODEL

The structure of the proposed artificial meta-atom in a Kekulé lattice is shown in Fig. 1(a), where the black solid hexagons embedding six cylindrical pillars in dark blue are the original units of a Kekulé lattice. An odd parity for spatial inversion exists at the Brillouin zone Γ point of the Kekulé
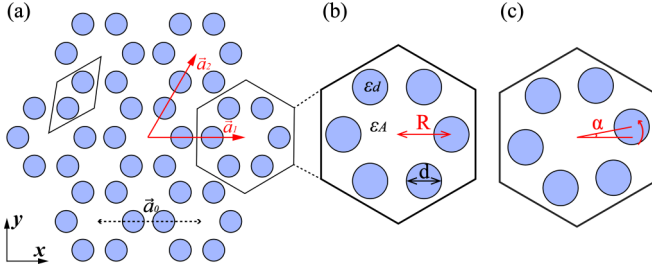
FIG. 1. Schematic diagram of a two-dimensional (2D) Kekulé lattice with a lattice constant of a_0. (a) The arrangement of the lattice unit marked by the black solid line and the lattice red vectors. (b) Unit cell before rotation. (c) Unit cell under a rotation angle $\alpha = 9.4°$.

unit, and also double-degenerate Dirac cones occur [3,23]. Therefore, with the hexagon in the composition of the triangular lattice, a_0 is the lattice constant and $\mathbf{a}_1$ and $\mathbf{a}_2$ are unit vectors. The geometric parameters used in the model throughout this Letter are $a_0 = 1$, $a_0/R = 2.92$, $d = 0.11a_0$ unless otherwise stated. The outstanding pillars are made of yttrium iron garnet (YIG) material ($\varepsilon_d = 11.7$) and the background media is set as air. In the enlarged view in Fig. 1(b) of the hexagonal cluster, R is the length from the center of the hexagon to the center of the cylinder, and d is the diameter of the cylindrical pillars. For the rotation mechanism, Fig. 1(c) shows the diagram of the supercell when the cylindrical pillars rotate simultaneously for an angle of $\alpha = 9.4°$, clockwise around the center of the hexagon.

In order to facilitate the description of the topological phase transition mechanism, we consider the behavior of the transverse magnetic (TM) mode in a Kekulé PC with C_6 symmetry [8]. According to Maxwell's equation, the propagation of time-harmonic TM waves in PC can be described by [3]

$$\left[\frac{1}{\varepsilon(\mathbf{r})}\nabla \times \nabla \times\right]E_z(\mathbf{r})\hat{z} = \frac{\omega^2}{c^2}E_z(\mathbf{r})\hat{z}, \qquad (1)$$

where $\varepsilon(\mathbf{r})$ is the dielectric parameter and c the speed of light. When $\varepsilon(\mathbf{r})$ is periodic, the Bloch theorem applies in the form of EM waves.

For the representations of the $\mathbf{E}_z$ field at the Γ point, artificial atoms carry orbitals p_x (p_y) and d_{xy} ($d_{x^2-y^2}$), in analogy to the electron orbitals for a periodic array of atoms in a solid. Since a direct counterpart of the spins does not occur naturally, two eigenvectors $\mathbf{E}_1$ and $\mathbf{E}_2$ can be constructed as $[p_+, p_-]$ and $[d_+, d_-]$ (cf. Sec. I of Supplemental Material [25]), in which

$$p_\pm = \frac{p_x \pm ip_y}{\sqrt{2}}, \quad d_\pm = \frac{d_{x^2-y^2} \pm id_{xy}}{\sqrt{2}}. \qquad (2)$$

Here, the antiunitary operator $T = UK$ is proposed where $U = -i\sigma_y$, and K is a complex conjugate operator [3,15,18]. Since $U^2 = -1$ guarantees $T^2 = -1$, T can be used as a pseudo-TR operator in our photonic system. Under the action of the T operator, $[p_+, p_-]$ has the following transformations [18],

$$T^2 p_\pm = -p_\pm. \qquad (3)$$

Obviously, this pseudo-TR resulting from the crystal symmetry [3,23,26] plays the central role in our analog QSHE.

In other words, since pseudo-TR symmetry and pseudo-spin depend on C_6 symmetry, photons with pseudo-spins in the C_6 system will produce Kramer's degeneracy. It is worth clarifying that C_6 plus time-reversal symmetry is a true combination of protection degeneracy, and the TR operator is not the main basis for providing the system Kramer's degeneracy.

In an analog electronic system [23], the two eigenstates of odd parity in the photonic system can be represented by p_+ and p_- corresponding to the p-band pseudo-spin-up and pseudo-spin-down states. Similarly, the two states of even parity in $d_\pm$ can be mapped as the pseudo-spin-up and pseudo-spin-down states for the d band.

According to the $\mathbf{k} \cdot \mathbf{p}$ theory [27], an effective photonic Hamiltonian under the representation of $[p_+, \quad d_+, \quad p_-, \quad d_-]^T$ is (cf. Sec. II of Supplemental Material [25])

$$H_0 = \begin{bmatrix} \omega_p^2/c^2 & Ak_+ & 0 & 0 \\ A^*k_- & \omega_d^2/c^2 & 0 & 0 \\ 0 & 0 & \omega_p^2/c^2 & A^*k_- \\ 0 & 0 & Ak_+ & \omega_d^2/c^2 \end{bmatrix}. \qquad (4)$$

In Eq. (4), $k_\pm = k_x \pm ik_y$, A is the coupling coefficient between the p and d states, and ω_p and ω_d the eigenfrequencies of the p band and d band, respectively. Note that in a C_6 symmetric system, only p states (d states) with the same spin direction can be coupled and Eq. (4) is similar to the electronic Hamiltonian in the Bernevig-Hughes-Zhang (BHZ) model [28–30], where the two block matrices correspond to the massive Dirac equations with pseudo-spin-up and pseudo-spin-down, respectively. This pair of pseudo-spin pairs are interconnected by an inversion symmetry operation, along with their disparate parities which ensures that the entire system satisfies pseudo-TR symmetry. If the p band is compared to the valence band and the d band to the conduction band [cf. Fig. 2(c)] analogous to the BHZ model in the electronic system, Eq. (4) serves as a Hamiltonian matrix of PQSHE. Then the topological state of our system should be determined as follows [24]. When $\omega_p > \omega_d$, the system corresponds to topological nontrivial states; when $\omega_p < \omega_d$, the system has parity inversion at the Γ point, which directly indicates the topological trivial state; when $\omega_p = \omega_d$, at the Γ point there occurs a band of fourfold degeneracy, corresponding to the double Dirac point which marks the transition point of topological phases [11].

III. RESULTS AND DISCUSSION

In this work, COMSOL software based on the finite-element method is used to calculate the PC dispersion and the electric field diagram. Considering the TM mode ($\mathbf{E}_z$, $\mathbf{H}_x$, and $\mathbf{H}_y$ components only), the band degeneracy and its breaking at the Γ point are achieved by adjusting the rotation angle of hexagons in every unit [31,32]. As show in Fig. 2, when the rotation angle is $12°$, the two degenerate bands split in proximity of the Γ point.

Based on the above theory, two degenerate band eigenstates are analogous to the quantum electron wave functions for the p band (blue solid line) and d band (red dotted line) [3,33]. According to the $\mathbf{E}_z$ fields in Figs. 2(d) and 2(e), we recognize that the dipole electric field belongs to the p band
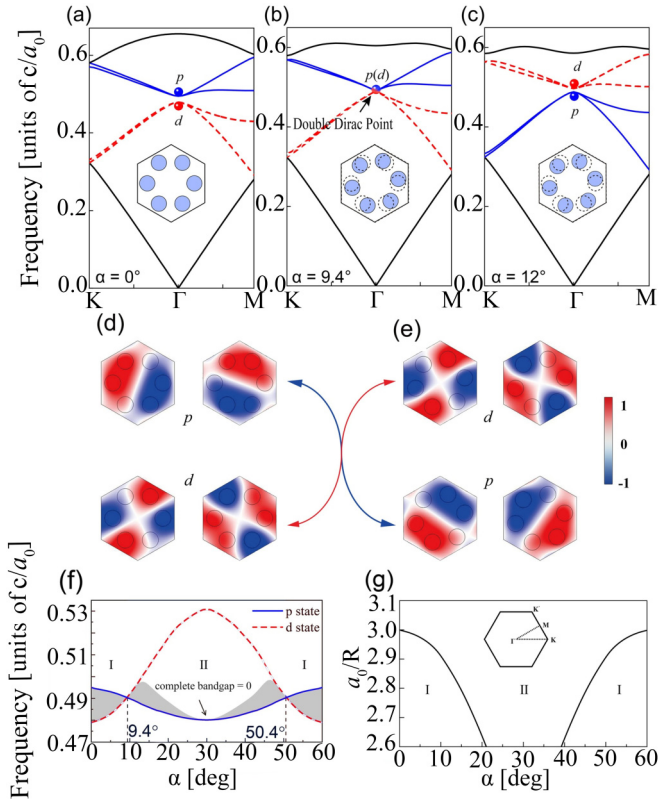
FIG. 2. TM mode dispersion diagrams (a)–(c) and eigenstate distribution (d) when the PC unit cells rotate for different angles. (a) Rotation angle $\alpha = 0°$. (b) $\alpha = 9.4°$ where band inversion (red dotted line and blue solid line represent the d band and p band) occurs to generate an accidental Dirac point. (c) $\alpha = 12°$. (d) E_z field of the p band and d band in (a). (e) E_z field of the d band and p band in (c). The black dashed lines in (b) and (c) indicate the unrotated unit cell. (f) Working frequency for rotation angle α with $a_0/R = 2.92$. The two regions I and II represent two different topological states of PC: I is the topological nontrivial phase, and II the trivial one. The shaded region represent the band-gap width. (g) Phase diagram with rotation angle α and lattice constant a_0/R (inset: the first Brillouin zone of the Kekulé lattice).

and the quadrupole one to the d band [34]. Therefore, the type of energy band can be determined according to the E_z fields. In Fig. 2(a), when the pillars are unrotated $\alpha = 0$, there are two degenerate points in each band. By observing the eigenfrequencies of the E_z fields, we find that the p band goes above the d band across the band gap. Here, in Fig. 2(a) our system is initially in a topological nontrivial state ($\omega_p > \omega_d$, represented by phase I). When the unit cell is rotated counterclockwise by 9.4° ($\alpha = 9.4°$), the eigenfrequency $\omega_p = \omega_d$ at the Dirac point Γ in Fig. 2(b) [11]. When we continue to adjust the rotation angle to $\alpha = 12°$, as shown in Fig. 2(c), the fourfold degeneracy point at the Γ point reopens. We then realize the band degeneracy and its breaking via a simple rotation of the unit cell. Figure 2(c) also indicates that the p band goes under the d band in contrast with Fig. 2(a) where the p and d bands are reversed at the Γ point, reducing it to a topologically trivial state ($\omega_p < \omega_d$, represented by phase II). The physical reason for topological phase switching results both from the band

inversion due to broken spatial inversion symmetry and also from the parity inversion [4,23].

The eigenfrequencies of the p and d bands within a period for 60° changes along with rotation angle α, as shown in Fig. 2(f). We find that the p and d bands reverse twice in one period of α, which occurs at both $\alpha = 9.4°$ and 50.4° as the topological phase transition points. Moreover, the complete band gap produced by the rotation mechanism increases to a peak at $\alpha = 13°$ and then becomes narrow along with an increasing rotation angle, and eventually vanishes for 30°. Furthermore, the first topological phase transition angle monotonically decreases with the relative lattice constant a_0/R, shown as the solid curve in Fig. 2(g). When a_0/R reaches 2.6, the neighboring atoms become tangent, which hinders designers to tune a_0/R further. In short, the rule of thumb for setting up parameters to achieve a topological phase indicates a range of $a_0/R = 2.6$–3, when the rotation angle of the unit cell can be tuned to close and open the topological band gap resulting from band inversion. It is worth noting that for $a_0/R > 3.0$ in the trivial phase II, any angle of rotation will not cause phase switching though a topologically trivial band gap still occurs near Γ point. Note that the rotation mechanism preserves the pseudo-TR of the system (cf. Sec. III of Supplemental Material [25]), and eases the method to generate the topological band gap without using magnetic experimental setups [3,15,35].

The hallmark of topological bands is the scattering-free boundary states propagating on the interfaces between distinct topological matters [3,15,35]. To reveal the edge states explicitly in our QSHE system, we plot the projected band dispersion and electric field E_z in a ribbon-shaped supercell composed of two distinct PCs, respectively $\alpha = 0°$ and $\alpha = 12°$ in Fig. 3. As the dispersion diagram in Fig. 3(a) shows, a pair of edge modes (represented by the red dot A and blue dot B) are observed within the band gap. This pair of edge states is topologically protected by pseudo-TR symmetry, which can be identified as the spin-up and spin-down modes. Actually, there is a tiny gap at the Γ point in Fig. 3(a) [unnoticeable in the present scale] due to the symmetry of C_6 being damaged to a certain extent at the interface between the two crystals. However, compared to the large size of the two crystals, C_6 symmetry could be taken as approximately kept and our topological properties maintained (cf. Sec. IV of Supplemental Material [25]). In the left panel of Fig. 3(b) we plot that the electric fields of the edge state for points A and B at k_x are ± 0.02 in units of $2\pi/a_0$ in Fig. 3(a). The field maps indicate the robust topologically protected edge states along the interface. In the two zoom-ins in the right panel of Fig. 3(b), the two circular arrows (red and blue for clockwise and counterclockwise rotation) indicate time-averaged power flow directions of $\mathbf{S} = \text{Re}[\mathbf{E} \times \mathbf{H}^*]/2$ for the edge states duo [36]. It demonstrates the helical edge states under spin-momentum locking explicitly.

To further validate the robust one-way propagation of topological helical edge states subject to PC defects [10,16], we use the helicity feature, i.e., the direction of the pseudo-spins, of the edge states to control the propagation of electromagnetic waves. The pseudo-spin-up (pseudo-spin-down) mode is selectively excited by using a positive (negative) circular polarization excitation source S_+ (S_-) [3]. On the interface
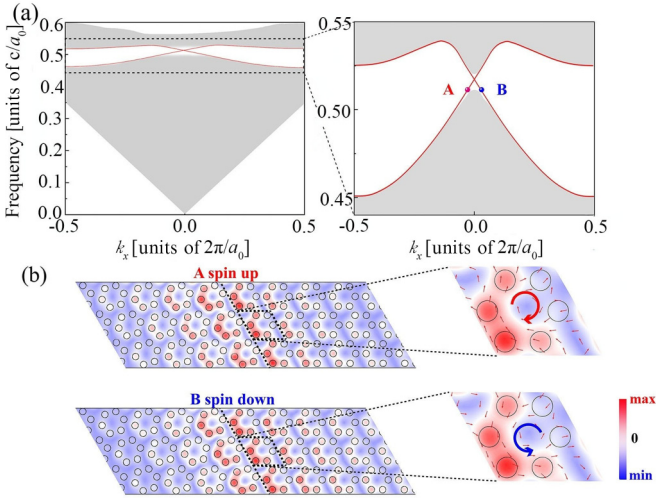
FIG. 3. (a) Projected band diagram of a one-dimensional super-cell, composed of both a topologically nontrivial phase I ($\alpha = 0°$) and topologically trivial phase region II ($\alpha = 12°$). A (red dot) and B (blue dot) correspond to the clockwise spiral and counterclockwise helical edge states, respectively. (b) Left panel: Electric field distribution $\mathbf{E}_z(x, y)$ around the edge. Right panel: Zoom-ins for electric field $\mathbf{E}_z$. The arrows represent the average Poynting vector directions and the magnitude corresponding to points A and B for k_x is ±0.02, in units of $2\pi/a_0$, and circular thick arrows in red and blue are guides for the eyes.

of two kinds of photonic crystals with distinct topological phases, we observe the EM propagation mostly along the edge. In the waveguide design, we make use of the wider common band gap to excite the topological edge state selectively. For the topological nontrivial (I) part the parameters are kept the same as Fig. 3, while for the trivial phase (II) part, the parameters $a_0/R = 3$, $\alpha = 12°$ are chosen with other parameters unchanged. When the working frequency is chosen as 0.52 in units of c/a_0, the in-line waveguide excites EM waves by the pseudo-spin source S_+. Simulation shows that these edge states can transmit EM waves well in the selected rightward direction as shown in Fig. 4(a). To verify the defect immunity characteristics of the topological edge state, an in-line waveguide with defects is designed as shown in Fig. 4(b). Simulation also verifies that EM waves are still able to transmit around the disordered region to localize at the topological interface. Furthermore, to validate the backscattering immunity characteristics of the edge states, a Z-shaped waveguide with sharp bends is shown in Fig. 4(c). The EM wave excited from S_+ propagating along the Z-shaped interface between the topological distinct phases (II/I) can travel around the geometric bends without significant loss. In order to represent the energy flow in the waveguide excited by different chiral excitation sources, a Poynting vector distribution of the in-line waveguide and the defective waveguide are plotted in Figs. 4(d) and 4(e), which is distributed in a one-way transverse vortex during its propagation. By calculating the transmission efficiency of the three waveguides in Figs. 4(a)–4(c), as shown in Fig. 4(f), we confirm that the energy transmission of the waveguides around the band gaps I and II has negligible loss. In order to further verify the topological feature of the
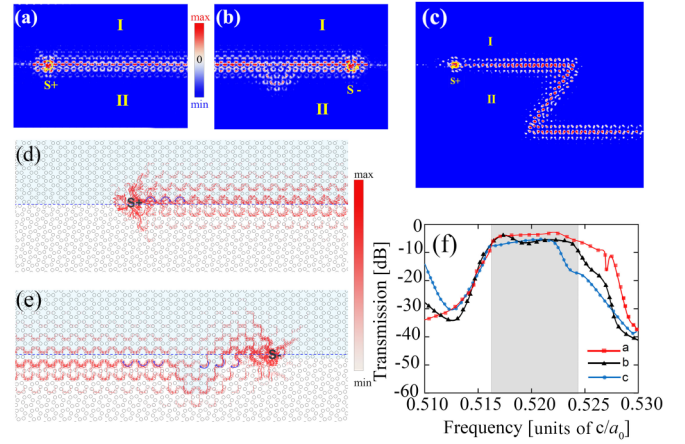

FIG. 4. A defect waveguide along the interface between two types of PCs (I: $\alpha = 0°$ and II: $\alpha = 12°$, $a_0/R = 3$). The positive (negative) circular polarization excitation source S_+ (S_-) represents the pseudo-spin-up (pseudo-spin-down) mode with frequency of 0.52 in units of c/a_0. (a) Electric field of the edge state is excited by the pseudo-spin-up mode S_+, showing that the EM wave propagates unidirectionally to the right. (b) In the presence of defects, the crystal lattice appears disordered on the interface between I and II and the spin-down mode is still able to excite reflectionless transmission. (c) On an interface with a sharp angle, EM waves can also steer around geometric bends without backscattering. (d) Poynting vector distribution of an in-line waveguide excited by the S_+ source. (e) Poynting vector distribution of the S_- source excited in a bent waveguide. (f) Transmission spectra measured around band gaps in gray I and II [lines with red squares, black triangles, and blue circles respectively represent the corresponding waveguides in (a)–(c)].

edge-state propagation, two boundary types of waveguides are designed, in which the zigzag boundary is used in Fig. 3 and the armchair-type boundary state also demonstrates backscattering suppression and null-interference properties (cf. Sec. V of Supplemental Material [25]). Our results confirm that the boundary states induced by our rotation-induced phase transition are a true analog of QSHE states, which are robust one-way reflectionless traveling eigenwaves against defects [3,15].

IV. CONCLUSIONS

In summary, based on the pure-dielectric Kekulé lattice, we use the synchronized rotation of the unit cells to induce a topological phase transition on a PC platform. The pseudo-TR symmetry is constructed based on the C_6 symmetry of the Kekulé lattice in design, and the topological phase transition in the rotation mechanism maintains the pseudo-TR inversion. Our model exploits the rotational freedom of the pillars to break the mirror symmetry of the crystal lattice, thereby reducing the manufacturing requirements to manipulate the Dirac points. The synchronized rotation of unit cells directly opens the band gap, providing an additional degree of freedom for the generation of a topological gap without magnetic experimental setups. Electromagnetic wave simulation verifies that topological edge states emerge within a band gap due to the synchronized rotation of unit cells. Other than the already-

known platforms [24,37–40], we hope that this work provides a design possibility for scrutinizing optical QSHE systems.

ACKNOWLEDGMENTS

[1] C. L. Kane and E. J. Mele, Quantum Spin Hall Effect in Graphene, Phys. Rev. Lett. **95**, 226801 (2005).

[2] L. Fu, Topological Crystalline Insulators, Phys. Rev. Lett. **106**, 106802 (2011).

[3] F. D. M. Haldane and S. Raghu, Possible Realization of Directional Optical Waveguides in Photonic Crystals with Broken Time-Reversal Symmetry, Phys. Rev. Lett. **100**, 013904 (2008).

[4] F. D. M. Haldane, Model for a Quantum Hall Effect without Landau Levels: Condensed-Matter Realization of the "Parity Anomaly", Phys. Rev. Lett. **61**, 2015 (1988).

[5] A. B. Khanikaev, S. H. Mousavi, and W.-K. Tse, Photonic topological insulators, Nat. Mater. **12**, 233 (2013).

[6] L. Lu and J. D. Joannopoulos, Topological photonics, Nat. Photonics **8**, 821 (2014).

[7] S. Hughes, L. Ramunno, J. F. Young, and J. E. Sipe, Extrinsic Optical Scattering Loss in Photonic Crystal Waveguides: Role of Fabrication Disorder and Photon Group Velocity, Phys. Rev. Lett. **94**, 033903 (2005).

[8] Z. Wang, Y. D. Chong, J. D. Joannopoulos, and M. Soljacic, Reflection-Free One-Way Edge Modes in a Gyromagnetic Photonic Crystal, Phys. Rev. Lett. **100**, 013905 (2008).

[9] Z. Wang, Y. Chong, J. D. Joannopoulos, and M. Soljacic, Observation of unidirectional backscattering-immune topological electromagnetic states, Nature (London) **461**, 772 (2009).

[10] M. He, L. Zhang, and H. Wang, Two-dimensional photonic crystal with ring degeneracy and its topological protected edge states, Sci. Rep. **9**, 3815 (2019).

[11] X. Q. Huang, Y. Lai, Z. H. Hang, H. H. Zheng, and C. T. Chan, Dirac cones induced by accidental degeneracy in photonic crystals and zero-refractive-index materials, Nat. Mater. **10**, 582 (2011).

[12] T. Xu, D. Zhu, and Z. H. Hang, Pulse reshaping in double-zero-index photonic crystals with Dirac-like-cone dispersion, Sci. Rep. **10**, 8416 (2020).

[13] Z. G. Chen, J. Mei, X. C. Sun, X. Zhang, J. Zhao, and Y. Wu, Multiple topological phase transitions in a gyromagnetic photonic crystal, Phys. Rev. A **95**, 043827 (2017).

[14] L. Xu, H. X. Wang, Y. D. Xu, H. Y. Chen, and J. H. Jiang, Accidental degeneracy in photonic bands and topological phase transitions in two-dimensional core-shell dielectric photonic crystals, Opt. Express **24**, 18059 (2016).

[15] C. Xu, Quantum spin Hall, triplet superconductor, and topological liquid on the honeycomb lattice, Phys. Rev. B **83**, 024408 (2011).

[16] M. Wang, W. Zhou, L. Bi, C. Qiu, and Z. Liu, Valley-locked waveguide transport in acoustic heterostructures, Nat. Commun. **11**, 6 (2020).

[17] Y. Yang, Y. F. Xu, T. Xu, H. X. Wang, J. H. Jiang, X. Hu, and Z. H. Hang, Visualization of a Unidirectional Electromagnetic Waveguide Using Topological Photonic Crystals Made of Dielectric Materials, Phys. Rev. Lett. **120**, 217401 (2018).

[18] L.-H. Wu and X. Hu, Scheme for Achieving a Topological Photonic Crystal by using Dielectric Material, Phys. Rev. Lett. **114**, 223901 (2015).

[19] M. Kim and J. Rho, Topological edge and corner states in a two-dimensional photonic Su-Schrieffer-Heeger lattice, Nanophotonics **9**, 3227 (2020).

[20] M. Kim, Z. Jacob, and J. Rho, Recent advances in 2D, 3D and higher-order topological photonics, Light: Sci. Appl. **9**, 130 (2020).

[21] M. Jung, Z. Y. Fan, and G. Shvets, Midinfrared Plasmonic Valleytronics in Metagate-Tuned Graphene, Phys. Rev. Lett. **121**, 086807 (2018).

[22] X. Wen, C. Qiu, J. Lu, H. He, M. Ke, and Z. Liu, Acoustic Dirac degeneracy and topological phase transitions realized by rotating scatterers, J. Appl. Phys. **123**, 091703 (2018).

[23] X. L. Qi and S. C. Zhang, The quantum spin Hall effect and topological insulators, Phys. Today **63**(1), 33 (2010).

[24] C. Z. Chang, J. Zhang, F. Xiao, S. Jie, and Q. K. Xue, Experimental observation of the quantum anomalous Hall effect in a magnetic topological insulator, Science **340**, 167 (2013).

[25] See Supplemental Material at http://link.aps.org/supplemental/10.1103/PhysRevA.104.L031502 for the details of pseudospin construction and theoretical analysis, topological phase before and after the rotating unit cells, and topological characteristics of the two boundary types.

[26] C. He, X.-C. Sun, X.-P. Liu, M.-H. Lu, Y. Chen, L. Feng, and Y.-F. Chen, Photonic topological insulator with broken time-reversal symmetry, Proc. Natl. Acad. Sci. USA **113**, 4924 (2016).

[27] G. Y. Wu, T. C. McGill, C. Mailhiot, and D. L. Smith, $k \cdot p$ theory of semiconductor superlattice electronic structure in an applied magnetic field, Phys. Rev. B **39**, 6060 (1989).

[28] B. A. Bernevig, T. L. Hughes, and S.-C. Zhang, Quantum spin Hall effect and topological phase transition in HgTe quantum wells, Science **314**, 1757 (2006).

[29] H. X. Zhu, T. T. Wang, J. S. Gao, L. Shuai, and G. L. Liu, Floquet topological insulator in the BHZ model with the polarized optical field, Chin. Phys. Lett. **31**, 030503 (2014).

[30] S. Juergens, P. Michetti, and B. Trauzettel, Screening properties and plasmons of Hg(Cd)Te quantum wells, Phys. Rev. B **90**, 115425 (2014).

[31] S. Johnson and J. Joannopoulos, Block-iterative frequency-

domain methods for Maxwell's equations in a planewave basis, Opt. Express **8**, 173 (2001).

[32] J. Laegsgaard, N. A. Mortensen, and A. Bjarklev, Mode areas and field energy distribution in honeycomb photonic bandgap fibers, J. Opt. Soc. Am. B **20**, 2037 (2003).

[33] W. T. Dixon, Construction of molecular orbital energy level diagrams by the method of progressive interactions of atomic orbitals, J. Chem. Soc., Faraday Trans. 2 **73**, 67 (1977).

[34] J. Yang, I. Makasyuk, A. Bezryadina, and Z. Chen, Dipole solitons in optically induced two-dimensional photonic lattices, Opt. Lett. **29**, 1662 (2004).

[35] Y. F. Geng, Z. N. Wang, Y. G. Ma, and F. Gao, Topological surface plasmon polaritons, Acta Phys. Sin. **68**, 224101 (2019).

[36] I. A. Litvin, A. Dudley, and A. Forbes, Poynting vector and orbital angular momentum density of superpositions of Bessel beams, Opt. Express **19**, 16760 (2011).

[37] G. Q. Liang and Y. D. Chong, Optical Resonator Analog of a Two-Dimensional Topological Insulator, Phys. Rev. Lett. **110**, 203904 (2013).

[38] W. J. Chen, S. H. Jiang, X. D. Chen, B. C. Zhu, L. Zhou, J. W. Dong, and C. T. Chan, Experimental realization of photonic topological insulator in a uniaxial metacrystal waveguide, Nat. Commun. **5**, 5782 (2014).

[39] A. B. Khanikaev, R. Fleury, S. M. Mousavi, and A. Alu, Topologically robust sound propagation in an angular-momentum-biased graphenelike resonator lattice, Nat. Commun. **6**, 8260 (2015).

[40] K. Fang, Z. Yu, and S. Fan, Realizing effective magnetic field for photons by controlling the phase of dynamic modulation, Nat. Photonics **6**, 782 (2012).